Available online at www.sciencedirect.com
ScienceDirect
Trans. Nonferrous Met. Soc. China 23(2013) 1356−1366
Transactions of Nonferrous Metals Society of China
www.tnmsc.cn

Effects of ball milling time on porous Ti−3Ag alloy and its apatite-inducing abilities

Le-gan HOU[1], Li LI[2], Yu-feng ZHENG[1,2]

1. Center for Biomedical Materials and Engineering, Harbin Engineering University, Harbin 150001, China;
2. Department of Materials Science and Engineering, College of Engineering, Peking University, Beijing 100871, China

Received 25 September 2012; accepted 10 March 2013

Abstract: Ti and Ag powders were mixed with different ball milling time (1, 2, 5 and 10 h) and sintered into porous Ti−3Ag alloys. The samples were treated with hydrothermal treatment, and their apatite-inducing abilities were further evaluated by immersion in modified simulated body fluid. The results indicate that the high surface energy brought by powder refinement leads to the decline of Ag, but promotes the oxidation of Ti during the sintering process. Meanwhile, the hydrothermal treated porous Ti−3Ag alloys prepared by the powders ball milled for 10 h possess the best apatite-inducing ability.

Key words: porous Ti−3Ag alloy; hydrothermal treatment; apatite-inducing ability; ball milling time

1 Introduction

Titanium and its alloys have been widely used as implant materials for load-bearing conditions because of their excellent mechanical properties and biocompatibility [1−4]. However, the mismatch in elastic modulus between Ti (90−105 GPa) and bones (0.3−30 GPa) leads to severe stress shielding, resulting in bone resorption [5−7]. To solve this problem, the methods including alloying with low modulus [8−10], composite materials [11−13], porous materials [14−16] have been investigated. Among them, porous titanium by introducing a porous structure to reduce the elastic modulus of Ti-based biomaterials has been considered the best way. Meanwhile, it has been reported that excellent osteointegration was achieved on implants with bioactive layer rather than a pure titanium alloy [17−19]. Thus, hydrothermal treatment as a useful way to modify the physical and chemical properties of material surface was conducted on porous Ti−3Ag alloys [20,21].

Compared with pure titanium, Ti−Ag alloy shows very nice corrosion and mechanical properties. Meanwhile, the alloy also exhibits antibacterial ability as the introduction of Ag element [22]. Thus, it has attracted researchers' attention in recent years. Studies also indicated that high Ag elemental concentration may lead to cell toxicity [23], which is harmful to biomaterials. However, when the Ag content is controlled between 0 and 4.5%, the cell toxicity of Ti−Ag alloy on rat fiber cell is very little, which can be ignored [24]. And associated with the formation of Ti−Ag alloy, as the solid solubility of Ag in titanium is very low [24], about 6% under 600 °C, Ti−3Ag alloy is a very suitable material for implant application.

A special powder metallurgy method was used to prepare the porous Ti−3Ag alloys [25]. The ball milling time is a key factor in powder refining [26], which directly affects the surface energy of the powders. In this work, four different ball milling time were used to prepare Ti−Ag alloy. The effect of ball milling time during powder metallurgy on porous Ti−3Ag alloys and its apatite-inducing ability in a modified simulated body fluid (SBF) were studied [27−29].

2 Experimental

2.1 Materials preparation

Porous Ti−3Ag alloys with 3% Ag were fabricated by powder metallurgy process with different ball milling

Foundation item: Projects (2012CB619102, 2012CB619100) supported by the National Basic Research Program of China; Projects (2011AA030101, 2011AA030103) supported by the High-tech Research and Development Program of China; Projects (HEUCFZ1017, HEUCFR1020) supported by the Fundamental Research Funds for the Central Universities, China; Project (ZD201012) supported by the Natural Science Foundation of Heilongjiang Province, China

Corresponding author: Yu-feng ZHENG; Tel: +86-10-62767411; E-mail: yfzheng@pku.edu.cn

DOI: 10.1016/S1003-6326(13)62604-7

time (1, 2, 5 and 10 h). Ti powder (purity, 99.4%) and Ag powder (purity, 99.9%) were used as the raw materials to prepare Ti−3Ag alloys, and urea particles were used as space-holding materials. First, raw powders and stainless steel balls (6 mm in diameter) in a mass ratio of 1:10 were put into stainless steel containers with the protection of Ar atmosphere. And then the mixed powders were milled in a planetary mill (QM-1SP04, China) with a rotation rate of 600 r/min at room temperature. After metallurgy process, urea particles sieved to 300−600 μm were mixed with ball-milled powders in a mass ratio of 1:1. The mixture was then cold compressed into compacts with a diameter of 20 mm in a stainless steel mould at 100 MPa for 5 min. The resultant compacts were heated to 250 °C for 1 h to burn out the spacer-holding particles in a vacuum furnace (1×10^{-2} Pa). Then, the porous green compacts were directly sintered at 1350 °C for 2 h in Ar atmosphere.

2.2 Hydrothermal treatment

During the hydrothermal treatment, the Ti−3Ag samples (10 mm×10 mm×1 mm) were immersed in 5.0 mol/L NaOH solution and kept at 60 °C for 24 h, then cleaned by fresh distilled water and dried at 40 °C. In the following, HT-Ti−3Ag represents the hydrothermal treated Ti−3Ag alloys.

2.3 Simulated body fluid immersion

The apatite-inducing ability was evaluated by soaking the porous HT-Ti−3Ag samples in simulated body fluid (SBF) (Table 1) at 37 °C for 7, 14 d respectively. And the SBF was refreshed every other day. NaCl, $NaHCO_3$, KCl, $K_2HPO_4\cdot3H_2O$, $MgCl_2\cdot6H_2O$, $CaCl_2$, and Na_2SO_4 were added into distilled water and buffered with Tris and 1.0 mol/L HCl at pH 7.40 to prepare SBF.

Table 1 Concentrations of reagent-grade chemicals for preparing SBF

Chemical	Concentration/(g·L^{-1})	Purity/%
NaCl	8.036	>99.5
$NaHCO_3$	0.352	>99.5
KCl	0.225	>99.5
$K_2HPO_4\cdot3H_2O$	0.230	>99.0
$MgCl_2\cdot6H_2O$	0.311	>98.0
$CaCl_2$	0.293	>96.0
Na_2SO_4	0.072	>99.0

2.4 Structure characterization

2.4.1 X-ray diffraction (XRD)

X-ray diffraction (XRD, D/max-γB, Japan) using Cu K_α radiation was used to analyze the surface phases of the porous Ti−3Ag alloys before and after hydrothermal treatment and after being incubated in SBF. The continuous scanning mode rate, current and accelerating voltage were set as 4 (°)/min, 50 mA and 40 kV, respectively.

2.4.2 Scanning electron microscope (SEM) and energy dispersive X-ray spectrometer (EDS)

Scanning electron microscope (SEM, Quanta 200, FEI Co., American) equipped with an energy dispersive X-ray spectrometer (EDS, EDAX, American) was used to observe the morphologies and detect elemental concentrations of the sample surfaces.

2.4.3 X-ray photoelectron spectroscopy (XPS)

To detect the chemical compositions of the sample surfaces, X-ray photoelectron spectroscopy (XPS, K-Alpha, Thermofisher Scienticfic Co., American) with Al K_α (1486.6 eV) X-ray source was used. And the vacuum, beam current, resolution scanning step and energy were set as 1.0×10^{-6} Pa, 6 mA, 0.1 eV and 0.5 eV, respectively.

2.4.4 Fourier transform infrared absorption (FT-IR) spectroscopy

Fourier transform infrared absorption spectroscopy (FT-IR, Bruker Vector 22, German) with a scanning range from 4000 to 400 cm^{-1} and resolution at 4 cm^{-1} was used to analyze the structure of the functional groups on the HT-Ti−3Ag alloys surface before and after SBF immersion. The surface coatings were scraped off from the sample, then mixed with KBr powder and pressed into transparent disks with a diameter of 13 mm for FT-IR works.

2.4.5 Materials characterization and mechanical test

The mass and dimensions of porous samples were measured to calculate the porosity. Accordingly, 6 samples from each group were weighed by a precision digital balance. Meanwhile, the digital caliper was used to measure the dimensions. Furthermore, to minimize the measurement error, both the height and diameter of cylindrical samples were measured at three different positions.

The universal materials testing machine (Instron 3365) was used to test the mechanical properties of as-sintered Ti−3Ag alloys at room temperature. The press head moving rate was set as 0.5 mm/min. And the tested samples were 10 mm-high cylinder with diameter of 8 mm. Five testing results for each kind of sample were calculated to get the mean value.

3 Results

3.1 Porous Ti−3Ag alloys

The morphologies of the milled powders with different ball milling time are shown in Fig.1. It is noticeable that the powders become finer with an even distribution of particle size with increasing ball milling time.

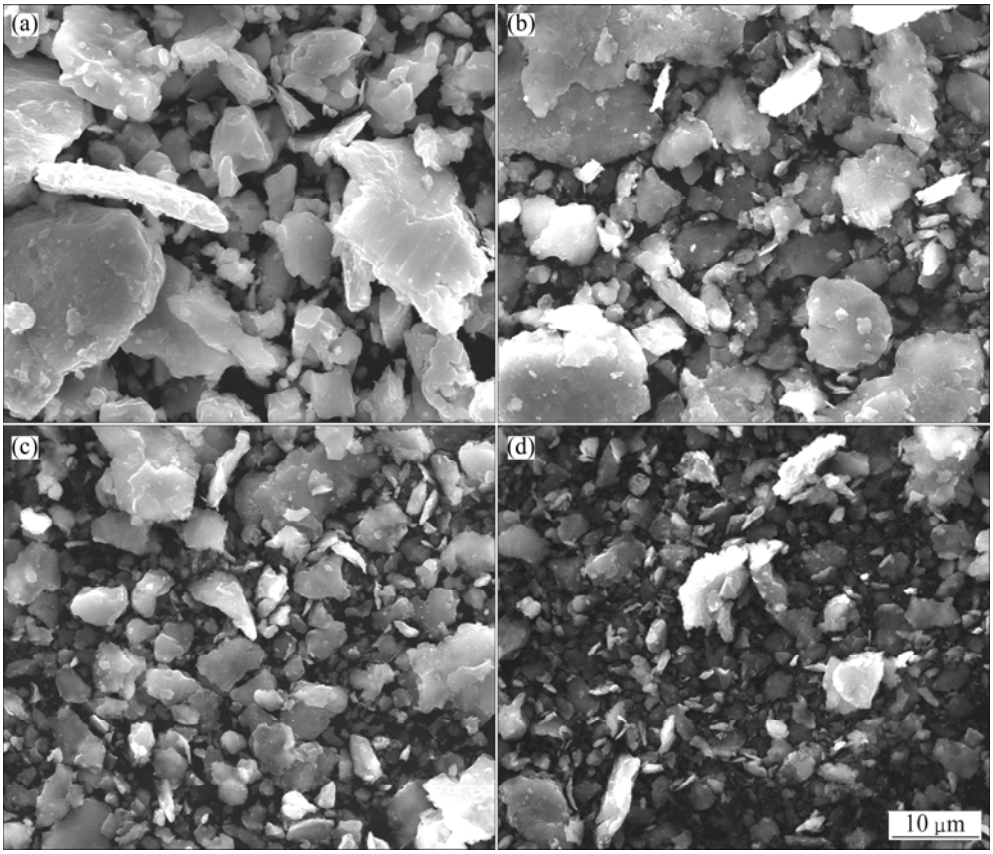

Fig. 1 SEM images of powders prepared with different ball milling time: (a) 1 h; (b) 2 h; (c) 5 h; (d) 10 h

Figure 2 shows the particle size distribution of those powders, where a significant change in particle size can be found. The particle size mainly gathered at two peaks. With the short ball milling time, the average powder size was 30 μm corresponding to the average particle size for raw Ti powders. But with increasing the ball milling time, much more powders were refined to 2 μm. Moreover, when the ball milling time lasted for 10 h, only one peak near 2 μm could be observed, indicating that almost all the powders were refined.

Figures 3 and 4 show the XRD patterns of the milled powders and as-sintered porous Ti−3Ag alloys, respectively. No reaction happened during the ball milling process (Fig. 3). Hence, the changes occurred after sintering. Instead of Ag, the peaks corresponding to TiO are found in Fig. 4. It was noticeable that the peak intensity of TiO increased greatly for the as-sintered porous Ti−3Ag alloys with the ball milling time increasing. After 10 h ball milling, the sample mainly consisted of TiO, without any pure Ti and Ag left. The

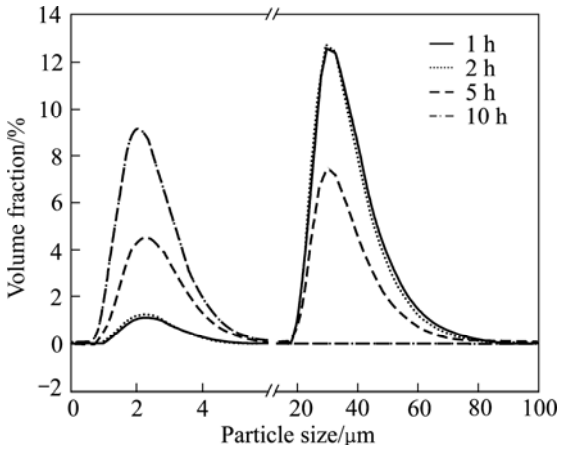

Fig. 2 Particle size distribution of powders prepared with different ball milling time

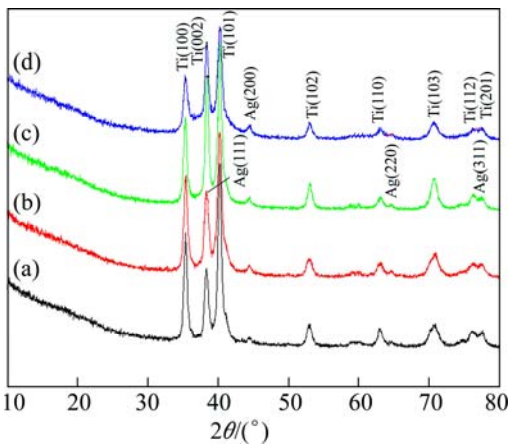

Fig. 3 XRD patterns of powders prepared with different ball milling time: (a) 1 h; (b) 2 h; (c) 5 h; (d) 10 h

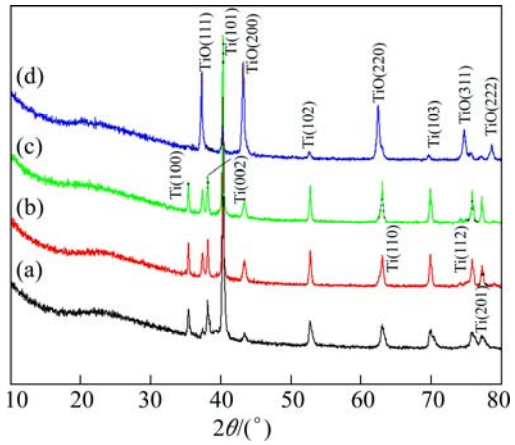

Fig. 4 XRD patterns of as-sintered porous Ti−3Ag alloys prepared by powders ball milled with different time: (a) 1 h; (b) 2 h; (c) 5 h; (d) 10 h

oxidation reaction was the result of low vacuum furnace (1×10^{-2} Pa) during the process of burning out the spacer-holding particles. As the oxygen had plenty time to react with sufficient Ti at a certain temperature, TiO was generated.

The SEM images of the as-sintered porous Ti−3Ag alloys with different ball milling time are shown in Fig. 5. The pores with size of (350±150) μm were open and interconnected throughout all the samples. Meanwhile, the pore walls also had pores with several microns in width, which were fabricated by sintering neck. However, no sintering neck could be observed from the pore walls of as-sintered porous Ti−3Ag alloys with 10 h ball milling time as the high surface energy promoted the densifying of the pore walls during the solid phase sintering.

The porosities of the as-sintered porous Ti−3Ag alloys with different ball milling time are listed in Table 2. It is interesting that the porosity decreases with the increasing ball milling time. This suggests that ball milling may play a promoting role in densification of the as-sintered porous Ti−3Ag alloys with the increasing surface energy caused by powder refinement, which is consistent with the results in Fig. 5. Table 2 also shows the mechanical properties of as-sintered porous Ti−3Ag alloys prepared with different ball milling time. With the decrease of bulk porosity, the compression strength and modulus increase dramatically. The compression strength varies from 15.7 MPa to 53.6 MPa. Meanwhile, it is noticeable that the elastic modulus of Ti−3Ag alloy is ranging from 1.0 GPa to 1.9 GPa, which is very familiar with the modulus of spongy bones. This indicates that

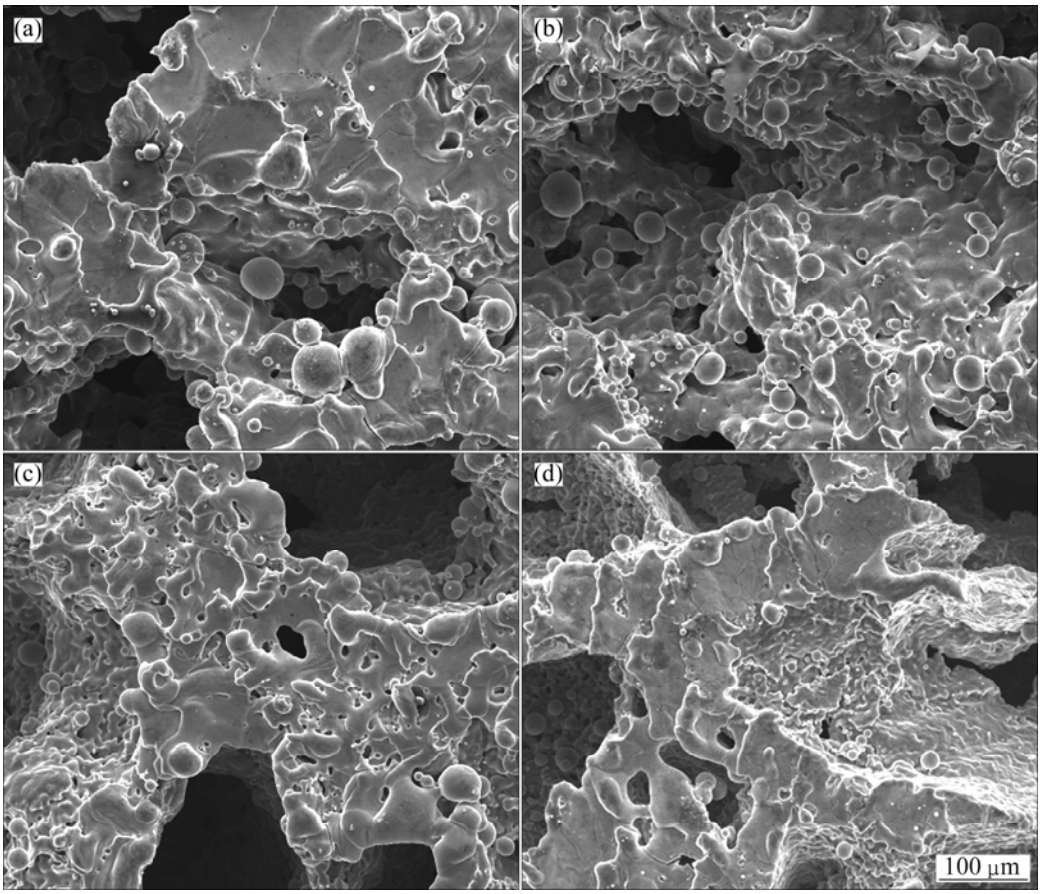

Fig. 5 SEM images of as-sintered porous Ti−3Ag alloys prepared by powders with different ball milling time: (a) 1 h; (b) 2 h; (c) 5 h; (d) 10 h

Table 2 Porosity and mechanical properties of Ti−3Ag alloys prepared with different ball milling time

Ball milling time/h	Porosity/ %	Compression strength/MPa	Elastic modulus/GPa
1	64.3±2.1	15.7±3.4	1.0±0.1
2	63.5±1.8	19.3±3.8	1.1±0.1
5	62.6±1.6	25.7±3.1	1.2±0.1
10	53.7±3.3	53.6±4.8	1.9±0.1

Ti−3Ag alloy is a very suitable material for implant application, for the familiar modulus can solve the stress shielding problem caused by mismatch of modulus.

3.2 Hydrothermally treated porous Ti−3Ag alloys

Figure 6 shows the XRD patterns of the hydrothermalloy treated porous Ti−3Ag alloys. No differences could be observed between the XRD results before and after hydrothermal treatment, because only a submicro porous layer was formed on the pore wall surface of the samples, as shown in Fig. 7. After analyzing the element contents of the samples surface before and after hydrothermal treatment (Table 3), it was found that sodium was introduced into the sample surfaces. Meanwhile, with the increasing ball milling time, the content of O element increased dramatically with the decrease of Ag and Na contents after the hydrothermal treatment.

Figure 8 shows the EDS surface scanning analyses. It is confirmed that Ti, O and Ag exist in the porous HT-Ti−3Ag alloys and distribute evenly.

XPS spectra indicate the chemical difference between the surface and the hydrothermally treated sample. Similar with the EDS results in Table 3, the elements Ag, Ti, O and Na can be detected from the surface (Fig. 9). The Ti 2p spectra reveal that the

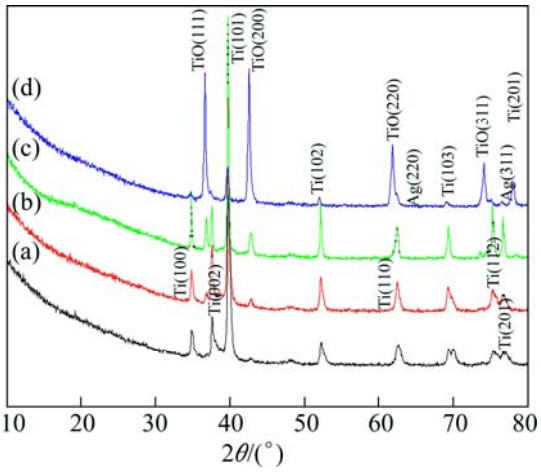

Fig. 6 XRD patterns of hydrothermally treated porous Ti−3Ag alloys prepared by powders with different ball milling time: (a) 1 h; (b) 2 h; (c) 5 h; (d) 10 h

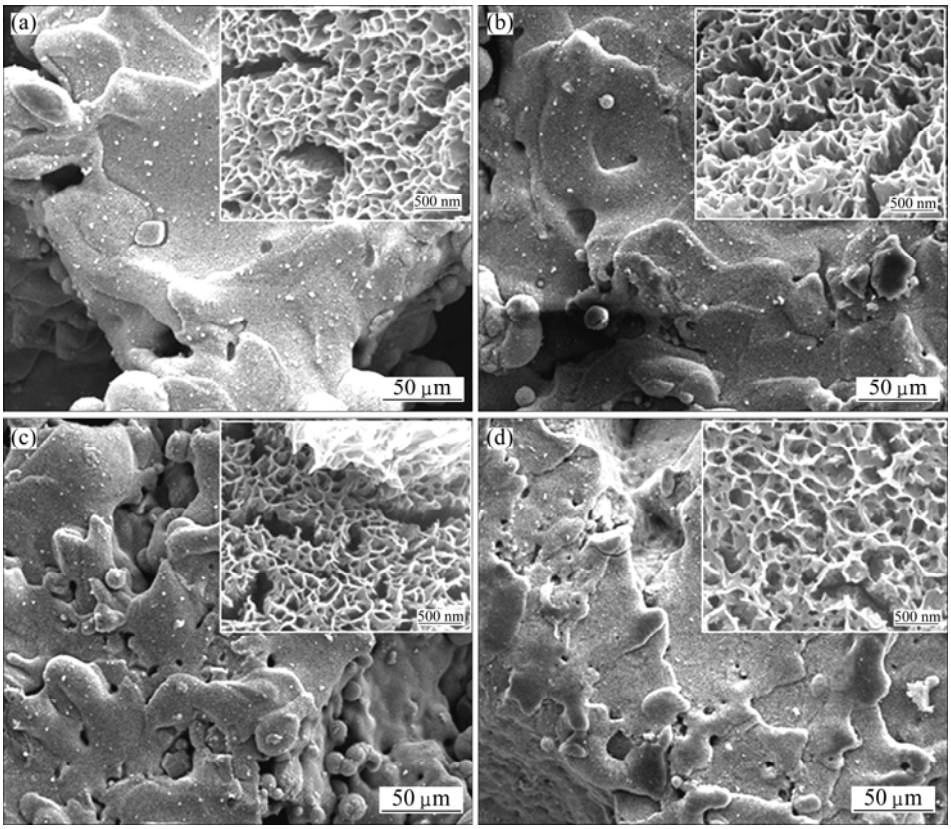

Fig. 7 SEM images of hydrothermal treated porous Ti−3Ag alloys prepared by powders with different ball milling time: (a) 1 h; (b) 2 h; (c) 5 h; (d) 10 h

Table 3 Element contents of surface of porous Ti−3Ag alloys before and after hydrothermal treatment (mass fraction, %)

Element	Before hydrothermal treatment				After hydrothermal treatment			
	1 h	2 h	5 h	10 h	1 h	2 h	5 h	10 h
Ti	71.11	68.54	67.92	70.11	57.23	56.00	54.2	58.06
O	26.22	28.28	30.13	29.43	38.85	40.39	42.45	40.89
Ag	2.67	3.18	1.95	0.46	1.93	1.96	1.71	0.42
Na	–	–	–	–	1.98	1.65	1.64	0.63

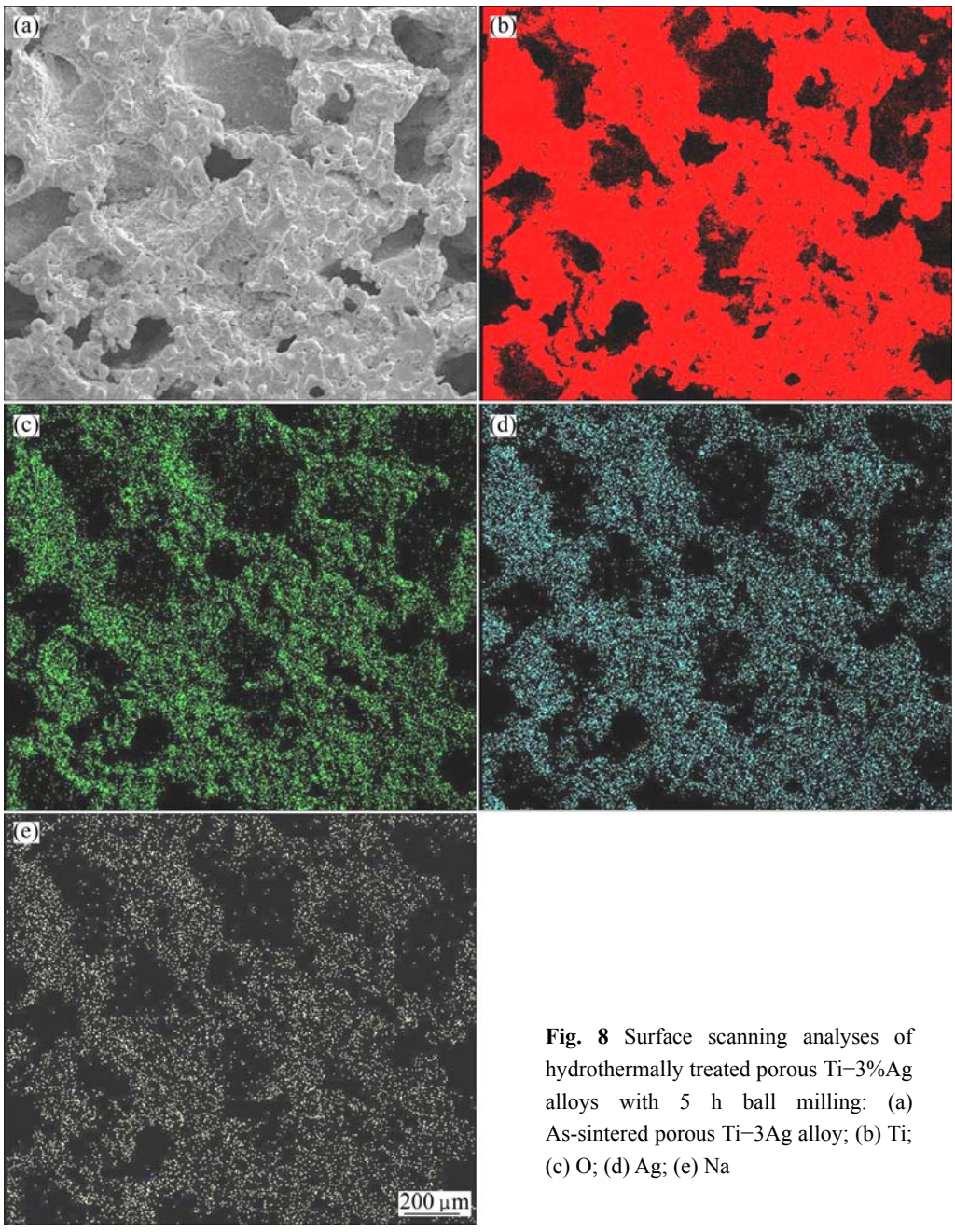

Fig. 8 Surface scanning analyses of hydrothermally treated porous Ti−3%Ag alloys with 5 h ball milling: (a) As-sintered porous Ti−3Ag alloy; (b) Ti; (c) O; (d) Ag; (e) Na

titanium exists as TiO_2 on the surface, and another peak corresponding to TiO_3^{2-} appears after etching (Fig. 10). Meanwhile, the O 1s spectra show that the oxygen exists as TiO_2 and basic hydroxyl $(OH)_b$ (Fig. 11). Furthermore, the Ag 3d spectra indicate that the silver exists as AgO and Ag_2O on the surface of samples. But in the sample with 10 h ball milling, Ag element disappears (Fig. 12).

3.3 Apatite-inducing ability of porous HT-Ti−3Ag alloys

Figures 13 and 14 show the XRD patterns of the porous HT-Ti−3Ag alloys with different ball milling time after being soaked in the SBF for 7 and 14 d, respectively. After 7 d immersion, no significant difference can be observed from Fig. 13. However, changes occurred after

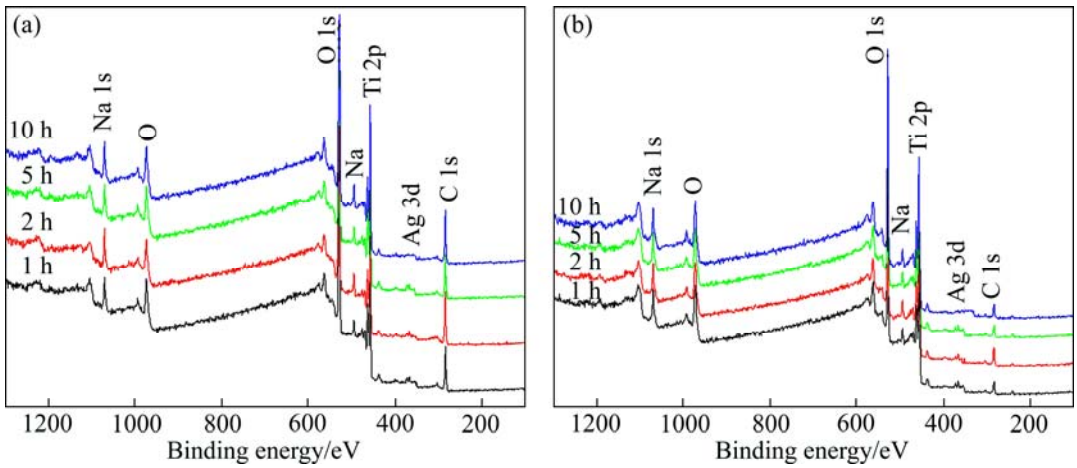

Fig. 9 XPS survey of hydrothermally treated porous Ti−3Ag alloys prepared by powders with different ball milling time before (a) and after (b) etching

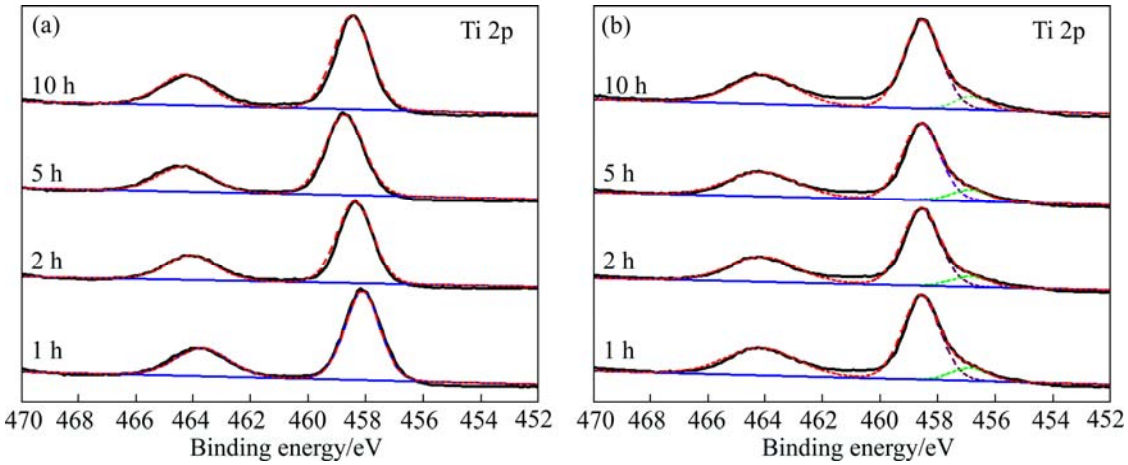

Fig. 10 XPS high-resolution spectra of Ti 2p of hydrothermally treated porous Ti−3Ag alloys prepared by powders with different ball milling time before (a) and after (b) etching

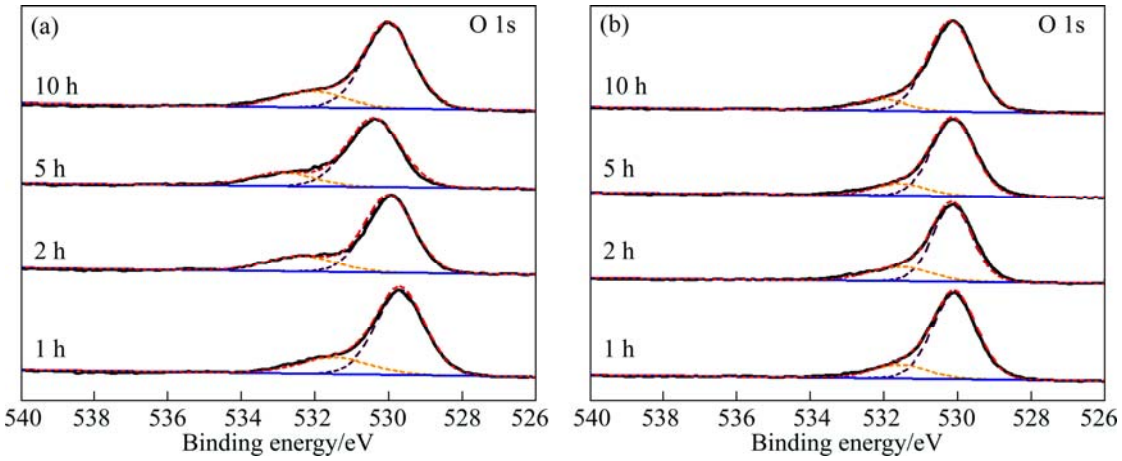

Fig. 11 XPS high-resolution spectra of O1s of hydrothermally treated porous Ti−3Ag alloys prepared by powders with different ball milling time before (a) and after (b) etching

another week soaking. Compared with the patterns of the porous HT-Ti−3Ag alloys in Fig. 13, those of samples in Fig. 14 display a number of relatively weak and broad peaks which can be marked as HA. The diffraction peaks of apatite indicate that the porous HT-Ti−3Ag alloys possess apatite-inducing ability. It is clear from the intensity of apatite diffraction peaks that porous HT-Ti−3Ag alloys with longer ball milling time have

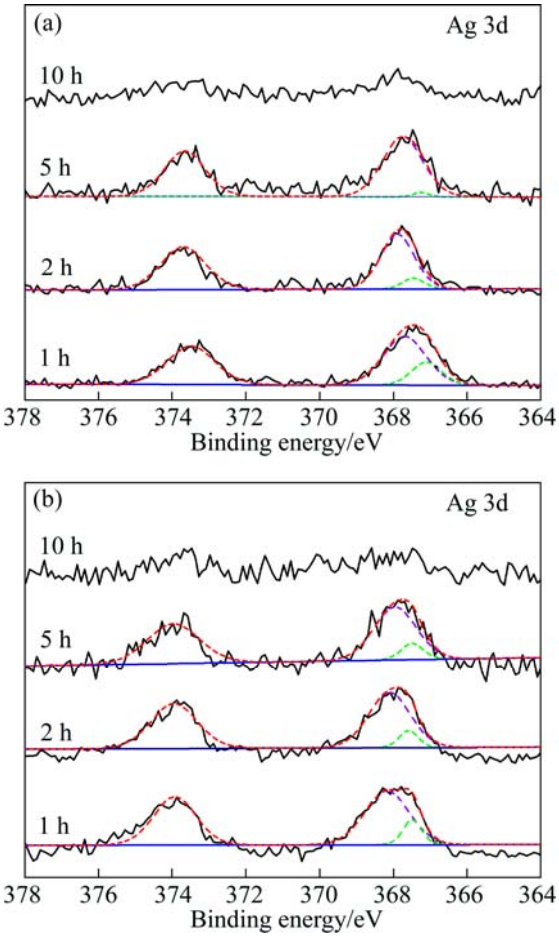

Fig. 12 XPS high-resolution spectra of Ag 3d of hydrothermally treated porous Ti−3Ag alloys prepared by powders with different ball milling time before (a) and after (b) etching

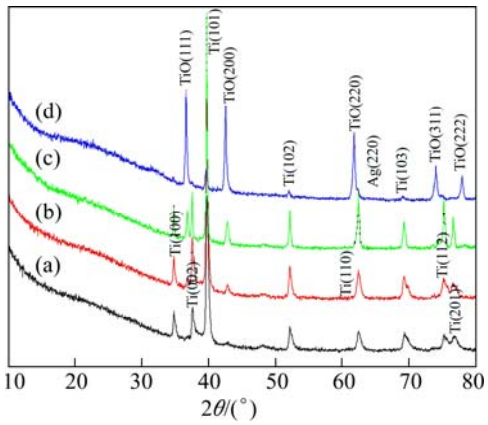

Fig. 13 XRD patterns of hydrothermally treated porous Ti−3Ag alloys prepared by powders with different ball milling time after SBF immersion for 7 d: (a) 1 h; (b) 2 h; (c) 5 h; (d) 10 h

better apatite-inducing ability.

Figures 15 and 16 show the SEM images of the porous HT-Ti−3Ag alloys after being soaked in SBF for 7 and 14 d, respectively. The results indicate that ball milling time has a significant effect on the apatite-inducing ability. Though apatite nucleation appears in the

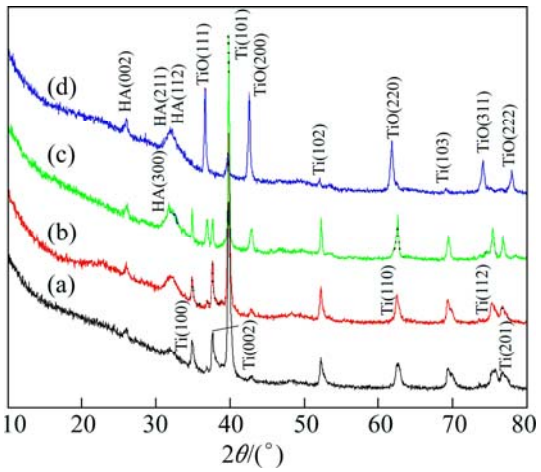

Fig. 14 XRD patterns of hydrothermally treated porous Ti−3Ag alloys prepared by powders with different ball milling time after SBF immersion for 14 d: (a) 1 h; (b) 2 h; (c) 5 h; (d) 10 h

porous HT-Ti−3Ag alloys at the same time (Fig. 15), much more HA is deposited on the samples with longer ball milling time but lower Ag content as shown in Fig. 16, which is well coinciding with the results in Fig. 14.

The FT-IR spectra of apatite coating formed on porous HT-Ti−3Ag alloys after SBF immersion for 14 d are shown in Fig. 17. Absorption peaks of PO_4 bands were observed including the triply degenerated asymmetric stretching mode of $\nu_3(PO_4)$ band at 1033 cm^{-1}, triply degenerated bending mode of $\nu_3(PO_4)$ band at 602 and 566 cm^{-1}. Meanwhile, the broad absorption band at 3441 cm^{-1} indicates the presence of $(OH)_b$ in the apatite coating. Thus, it confirms that the apatite formed on the porous HT-Ti−3Ag alloys is hydroxyapatite.

4 Discussion

4.1 Effect of ball milling time on surface phase composition after sintering

It has proved that the fine powders with higher surface energies can promote the sintering process with the decline of sintering potential energy. By increasing the ball milling time, the powder size decreases from 30 to 2 μm. Thus, the powders with higher surface energy obtain more energy for densifying during the same process. Meanwhile, the higher surface energy means that there is more energy for enhancing the oxidation reaction during the sintering process. Thereby, the sample with 10 h ball milling time mainly consists of TiO after sintering. Furthermore, the oxidation reaction between Ti and O releases large energy, leading to the sublimation of Ag element. By this way, the peaks corresponding to Ag cannot be found in the XPS results of the sample with 10 h ball milling time.

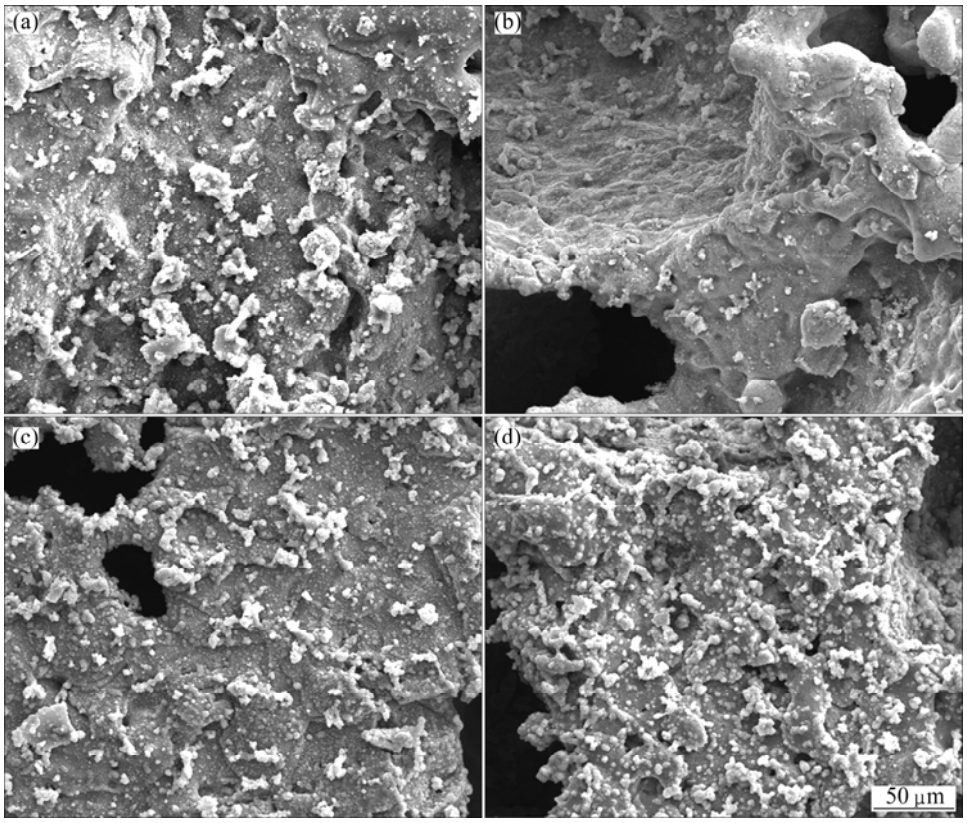

Fig. 15 SEM images of hydrothermally treated porous Ti−3Ag alloys prepared by powders with different ball milling time after SBF immersion for 7 d: (a) 1 h; (b) 2 h; (c) 5 h; (d) 10 h

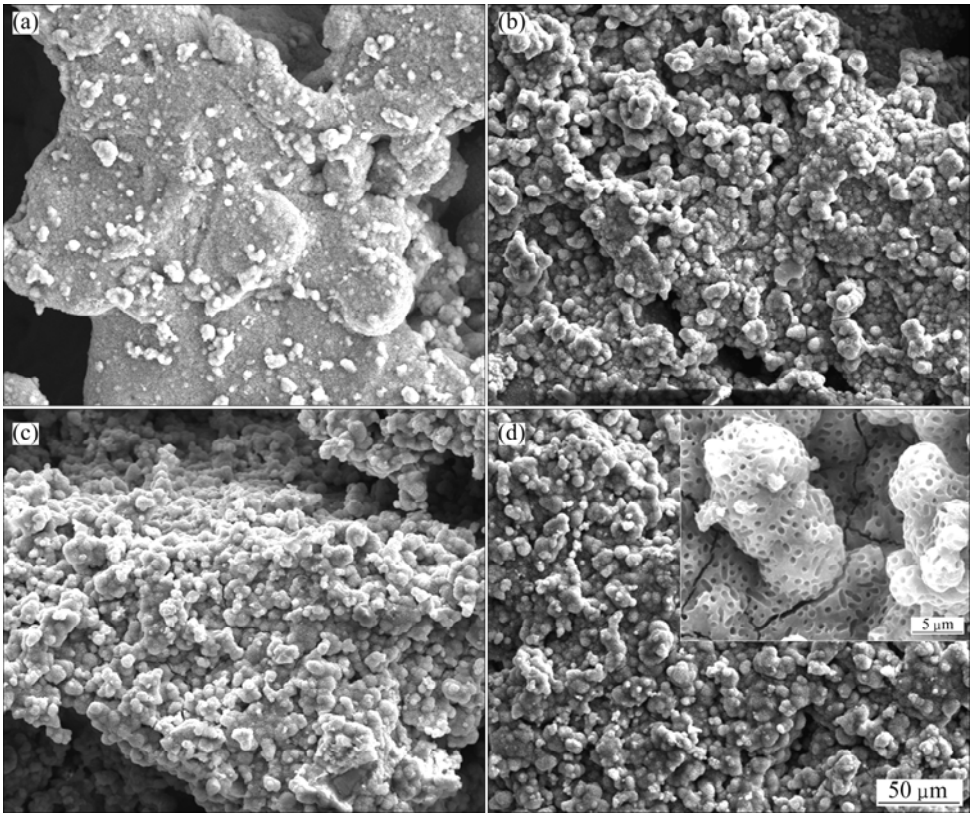

Fig. 16 SEM images of hydrothermally treated porous Ti−3Ag alloys prepared by powders with different ball milling time after SBF immersion for 14 d: (a) 1 h; (b) 2 h; (c) 5 h; (d) 10 h

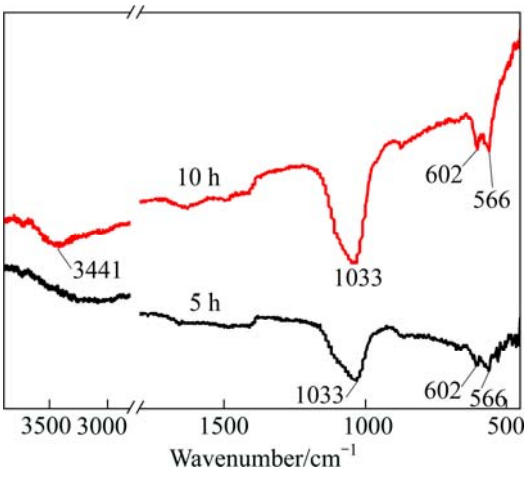

Fig. 17 FTIR spectra of hydrothermally treated porous Ti−3Ag alloys prepared by powders with different ball milling time after SBF immersion for 14 d

4.2 Effect of ball milling time on apatite-inducing ability

Considering the nucleation of HA, the process can be described as below. On the soaked sample surface, the TiO_3^- negative functional group is formed by releasing Na^+ ions. The negative charges caused by TiO_3^- on the porous HT-Ti−3Ag alloy surface might catch Ca^{2+} ions by Coulomb's force. Meanwhile, HPO_4^{2-} group and OH^- ions may also be attracted by the Ca^{2+} ions around the surface. As the enrichment of Ca^{2+}, HPO_4^{2-} and OH^- ions, HA can activate product according to the following equilibrium in SBF [30]:

$$10Ca + 6HPO_4^{2-} + 8OH^- \rightarrow Ca_{10}(PO_4)_6(OH)_2 + 6H_2O \quad (1)$$

Though the samples appear with HA nucleation at the same time, Ag ions with a strong oxidizing ability becomes the key point for the growth of HA. And basic hydroxyl $(OH)_b$ is another important factor in apatite-inducing ability [30,31]. As Ag ion can consume and control a large quantity of $(OH)_b$, it directly limits the apatite-inducing ability. Thus, the samples treated with longer ball milling time and little Ag content possess better apatite-inducing ability.

Based on the above facts, it seems that longer ball milling time provides the sintering powders with higher surface energy by powder refinement. The higher surface energy promotes the densifying of the sintered powders and formation of TiO as well as the sublimation of Ag element. With the decline of amount of Ag ions in the sample, HA can deposit on the sample surface much easily. Thus, the samples treated with longer ball milling time but with little Ag content possess better apatite-inducing ability.

5 Conclusions

1) The TiAg powders were realized at different ball milling time (1, 2, 5 and 10 h) to prepare porous Ti−3Ag alloys, and then they were sintered at 1350 °C for 2 h in Ar atmosphere. TiO was formed during the process of burning out the spacer-holding particles at the low vacuum furnace (1×10^{-2} Pa).

2) The samples were treated with hydrothermal treatment. The apatite-inducing ability of the hydrothermally treated porous Ti−3Ag alloys was evaluated in modified simulated body fluid. The results indicate that longer ball milling time provides the sintering powders with higher surface energy by powder refinement. The higher surface energy promotes the densifying of the sintered powders and the formation of TiO as well as the sublimation of Ag element.

3) With the decline of Ag ions amount in the sample, HA can easily deposit on the sample surface. Thus, the samples treated with longer ball milling time and little Ag content possess better apatite-inducing ability.

References

[1] CIMPEAN A, MITRAN V, CIOFRANGEANU C M. Osteoblast cell behavior on the new beta-type Ti−25Ta−25Nb alloy [J]. Materials Science and Engineering C, 2012, 32(6): 1554−1563.

[2] WEBSTER T J, EJIOFOR J U. Increased osteoblast adhesion on nanophase metals: Ti, Ti6Al4V, and CoCrMo [J]. Biomaterials, 2004, 25(19): 4731−4739.

[3] LONG M, RACK H J. Titanium alloys in total joint replacement—A materials science perspective [J]. Biomaterials, 1998, 19(18): 1621−1639.

[4] SHABALOVSKAYA S A. Surface, corrosion and biocompatibility aspects of nitinol as an implant material [J]. Bio-medical Materials and Engineering, 2002, 12(1): 69−109.

[5] HEDIA H S, ABDL-SHAFI A A, FOUDA N. The effect of elastic modulus of the backing material on the fatigue notch factor and stress [J]. Bio-medical Materials and Engineering, 2000, 10(3−4): 141−156.

[6] HEAD W C, BAUK D J, EMERSON R H Jr. Titanium as the material of choice for cementless femoral components in total HIP arthroplasty [J]. Clinical Orthopaedics and Related Research, 1995, (311): 85−90.

[7] CLIFT S E, FISHER J, WATSON C J. Finite element stress and strain analysis of the bone surrounding a dental implant: Effect of variations in bone modulus [J]. Proceedings of the Institution of Mechanical Engineers, Part H: Journal of Engineering in Medicine, 1992, 206(4): 233−241.

[8] BHOLA S M, BHOLA R, MISHRA B, OLSON D L. Povidone-iodine as a corrosion inhibitor towards a low modulus beta Ti−45Nb implant alloy in a simulated body fluid [J]. Journal of Materials Science—Materials in Medicine, 2011, 22(4): 773−779.

[9] GUILLEMOT F. Recent advances in the design of titanium alloys for orthopedic applications [J]. Expert Review of Medical Devices, 2005, 2(6): 741−748.

[10] NIINOMI M, AKAHORI T. Improvement of the fatigue life of titanium alloys for biomedical devices through microstructural

control [J]. Expert Review of Medical Devices, 2010, 7(4): 481−488.
[11] ZHENG Xue-bin, HUANG Min-hui, DING Chuan-xian. Bond strength of plasma-sprayed hydroxyapatite/Ti composite coatings [J]. Biomaterials, 2000, 21(8): 841−849.
[12] WEN C E, XU W, HU W Y. Hydroxyapatite/titania sol-gel coatings on titanium-zirconium alloy for biomedical applications [J]. Acta Biomaterialia, 2007, 3(3): 403−410.
[13] KHOR K A, GU Y W, QUEK C H. Plasma spraying of functionally graded hydroxyapatite/Ti−6Al−4V coatings [J]. Surface & Coatings Technology, 2003, 168(2−3): 195−201.
[14] LI B Y, RONG L J, LI Y Y. Synthesis of porous Ni−Ti shape-memory alloys by self-propagating high-temperature synthesis: Reaction mechanism and anisotropy in pore structure [J]. Acta Materialia, 2000, 48(15): 3895−3904.
[15] WEN C E, MABUCHI M, YAMADA Y. Processing of biocompatible porous Ti and Mg [J]. Scripta Materialia, 2001, 45(10): 1147−1153.
[16] RYAN G, PANDIT A, APATSIDIS D P. Fabrication methods of porous metals for use in orthopaedic applications [J]. Biomaterials, 2006, 27(13): 2651−2670.
[17] CHOU L, MAREK B, WAGNER W R. Effects of hydroxylapatite coating crystallinity on biosolubility, cell attachment efficiency and proliferation in vitro [J]. Biomaterials, 1999, 20(10): 977−985.
[18] AVNIR D, CORADIN T, LEV O. Recent bio-applications of sol-gel materials [J]. Journal of Materials Chemistry, 2006, 16(11): 1013−1030.
[19] FILIAGGI M J, COOMBS N A, PILLIAR R M. Characterization of the interface in the plasma-sprayed HA coating/Ti−6Al−4V implant system [J]. Journal of Biomedical Materials Research, 1991, 25(10): 1211−1229.
[20] YU Jia-guo, WANG Wen-guang, CHENG Bei, SU Bao-lian. Enhancement of photocatalytic activity of mesporous TiO_2 powders by hydrothermal surface fluorination treatment [J]. Journal of Physical Chemistry C, 2009, 113(16): 6743−6750.
[21] SUZUKI Y, YOSHIKAWA S. Synthesis and thermal analyses of TiO_2-derived nanotubes prepared by the hydrothermal method [J]. Journal of Materials Research, 2004, 19(4): 982−985.
[22] KANG M K, MOON S M, KWON J S, KIM K M, KIM K N. Antibacterial effect of sand blasted, large-grit, acid-etched treated Ti−Ag alloys [J]. Materials Research Bulletin, 2012, 47(10): 2952−2955.
[23] ZHANG B B, QIU K J, WANG B L, LI L, ZHENG Y F. Surface characterization and cell response of binary Ti−Ag Alloys with CP Ti as material control [J]. Journal of Materials Science & Technology, 2012, 28(9): 779−784.
[24] OH K T, SHIM H M, KIM K N. Properties of titanium-silver alloys for dental application [J]. Journal of Biomedical Materials Research, Part B, 2005, 74(1): 649−658.
[25] WEN C E, MABUCHI M, YAMADA Y. Processing of biocompatible porous Ti and Mg [J]. Scripta Materialia, 2001, 45(10): 1147−1153.
[26] SALAHINEJAD E, AMINI R, HADIANFARD M J. Effect of milling time on structure and mechanical properties of porous nickel-free austenitic stainless steels processed by mechanical alloying and sintering [J]. Materials Science and Engineering A, 2010, 527(21−22): 5522−5527.
[27] TANAHASHI M, MATSUDA T. Surface functional group dependence on apatite formation on self-assembled monolayers in a simulated body fluid [J]. Journal of Biomedical Materials Research, 1997, 34(3): 305−315.
[28] OYANE A, ONUMA K, ITO A. Formation and growth of clusters in conventional and new kinds of simulated body fluids [J]. Journal of Biomedical Materials Research, Part A, 2003, 64(2): 339−348.
[29] OYANE A, KIM H M, FURUYA T. Preparation and assessment of revised simulated body fluids [J]. Journal of Biomedical Materials Research, Part A, 2003, 65(2): 188−195.
[30] KIM H M, MIYAJI F, KOKUBO T, NAKAMURA T. Preparation of bioactive Ti and its alloys via simple chemical surface treatment [J]. Journal of Biomedical Materials Research, 1996, 32(3): 409−417.
[31] CHEN X, LI Y, DU P J, HODGSON P D, WEN C E. Influence of calcium ion deposition on apatite-inducing ability of porous titanium for biomedical applications [J]. Acta Biomaterialia, 2009, 5(5): 1808−1820.

球磨时间对多孔 Ti−3Ag 合金及其磷灰石诱导能力的影响

侯乐干[1]，李 莉[1]，郑玉峰[1,2]

1. 哈尔滨工程大学 生物医学材料与工程研究中心，哈尔滨 150001；
2. 北京大学 工学院 材料科学与工程系，北京 100871

摘 要：采用经不同球磨时间(1，2，5 和 10 h)混合的 Ti 和 Ag 粉末制备多孔 Ti−3Ag 合金，然后对该合金进行水热反应处理，并利用浸泡模拟体液研究其磷灰石诱导能力。结果表明，粉料细化能导致表面能增高和 Ag 含量降低，同时加快 Ti 在烧结过程中的氧化。经水热处理后，球磨 10 h 的多孔 Ti−3Ag 合金试样具有最优异的磷灰石诱导能力。

关键词：多孔 Ti−3Ag 合金；水热反应；磷灰石诱导能力；球磨时间

(Edited by Xiang-qun LI)